Density, Speed of Sound and other Derived Properties of Ethanol at Pressures up to 65 MPa

Pezhman Ahmadi [a], *Behzad Nezhad Karim Nobakht* [b], *Antonin Chapoy** [a,c]

[a] *Hydrates, Flow Assurance & Phase Equilibria Research Group, Institute of Petroleum Engineering, Heriot-Watt University, Edinburgh EH14 4AS, Scotland, UK*

[b] *Uncertainty Quantification Research Group, Institute of Petroleum Engineering, Heriot-Watt University, Edinburgh EH14 4AS, Scotland, UK*

[c] *Mines ParisTech, CTP – Centre Thermodynamique des procédés, 35 rue St Honoré 77305 Fontainebleau, France*

Abstract

A vibrating tube densitometer (VTD) and a high-pressure high-temperature (HPHT) acoustic cell were used to measure the density and speed of sound in ethanol for five isotherms at a temperature range of (323-423) K and pressures ranging up to 65 MPa. The measured sound velocities were used to calculate density and other derived properties employing the initial value method (IVM). The computed values were compared with the predictions of Schroeder et al.- equation of state for the thermodynamic properties of ethanol.

The overall average absolute deviations (% AAD) of the measured properties in comparison to predictions of the model were found to be 0.05 % and 0.30 % for the density and speed of sound, respectively. The overall expanded uncertainties (k=2) associated with the measured densities and sound velocities were found to be 0.03 % and 0.09 % respectively. Moreover, the overall % AAD of the calculated properties in comparison to the predicted values of the model were calculated to be 0.05 %, 0.74 %, 0.58 % and 3.16 % for density, isobaric and isochoric heat capacities and Joule-Thomson coefficient respectively. The overall expanded uncertainties (k =2) of the obtained properties were found to be 0.06 %, 0.04 %, 0.42 % and 0.32 % for density, isobaric and isochoric heat capacities and Joule-Thomson coefficient respectively.

1. Introduction

Due to its excellent ability to dissolve polar and non-polar substances, ethanol is the second most important solvent after water. It has a wide range of applications in the food and beverage, cosmetic, pharmaceutical, and chemical industries.[1-4]

Its extensive use in industrial applications means accurate knowledge of the thermodynamic properties of this fluid is essential for precise design and optimisation of industrial processes.

In 2004, the first fundamental equation of state (EoS) for the thermodynamic properties of ethanol was developed. [5] This model was established in the form of Helmholtz energy as a function of reduced temperature and density to predict thermodynamic properties at a temperature range of (250-650) K and pressures ranging up to 280 MPa. [5]

A decade later, employing the new reliable experimental results, the behaviour of the model in several areas, especially in the critical region, was improved. [6] Although the predicted thermodynamic properties of ethanol using the improved models were more accurate, observed deviations of the result in comparison with some of the reliable experimental data in the literature indicate shortcomings in the new model.[7-9]

Despite numerous investigations into the density of ethanol at different ranges of pressure and temperature (as shown in **Table 1**), experimental studies on the speed of sound in ethanol at high-pressure condition are scarce (as tabulated in **Table 2**). Among the available data in open literature, a few sets of measurement can be found at temperatures up to 350 Kand only a few data points are available at high temperature (T >500 K). Therefore, as depicted in **Figure 1**, a gap in the distribution of the existing data for the speed of sound in ethanol can be identified. For the isochoric and isobaric heat capacities, the available experimental results at high-pressure are limited to the works performed by Vega-Maza et al., Miyazawa et al. and Fulem et al. [10-12] Another investigation on the heat capacities of ethanol at high-pressure was carried out by Sun et al. [9, 13] Although a wide range of pressure (up to 280 MPa) was covered in their work, the temperature range was limited to the temperatures up to 333 K. To the best of our knowledge, for Joule-Thomson coefficient of ethanol no data are reported in the open literature.

The main objective of this study is to measure the density and speed of sound in ethanol simultaneously. The measured sound velocities were then used to obtain other derived properties of the fluid. Furthermore, the measured and calculated properties were compared with the predictions of the recent model developed by Schroeder et al. [6]

Table 1. Available high-pressure literature data for the density ρ of ethanol.

T/ K	*P* / MPa	Reference
308-358	Up to 15	[14]
293-673	0.098-245	[15]
273-363	2.76-22.1	[16]
298-328	37-208	[17]
298-348	0.1-196	[18]
200-500	1-50	[19]
373-673	0.224-40.3	[20]
297-483	Up to 57	[21]
263-483	0.1-56.7	[22]
310-363	0.015-200	[23]
310-480	Up to 200	[24]
308-384	0.014-14.9	[25]
283-418	5.74-28.9	[26]
298-348	0.1-40	[27]
283-353	0.1-45	[28]
293-333	0.1-65	[29]
283-343	0.1-35	[30]
278-353	0.1-35	[31]
283-328	Up to 20	[32]
233-473	Up to 30	[33]
303-323	0.1-10	[34]
250-333	Up to 70	[10]
278-353	Up to 70	[35]
283-328	Up to 40	[36]

Table 2. Literature data for the speed of sound *SoS* in ethanol at high-pressure.

Temperature/ K	Pressure / MPa	Reference
298	0.101-3190	[37]
303	0.098-196	[38]
293-318	0.101-91.5	[39]
303	0.098-479	[40]
193-263	0.101-276	[13]
274-333	0.101-275	[9]
294-299	4730-11000	[41]
293	49 & 98	[42]
273-323	0.101-96.5	[43]
518 & 543	3-50	[44]
253.2-353.2	0.101-30	[7]
298	0.101-3190	[37]
303	0.098-196	[38]
293-318	0.101-91.5	[39]

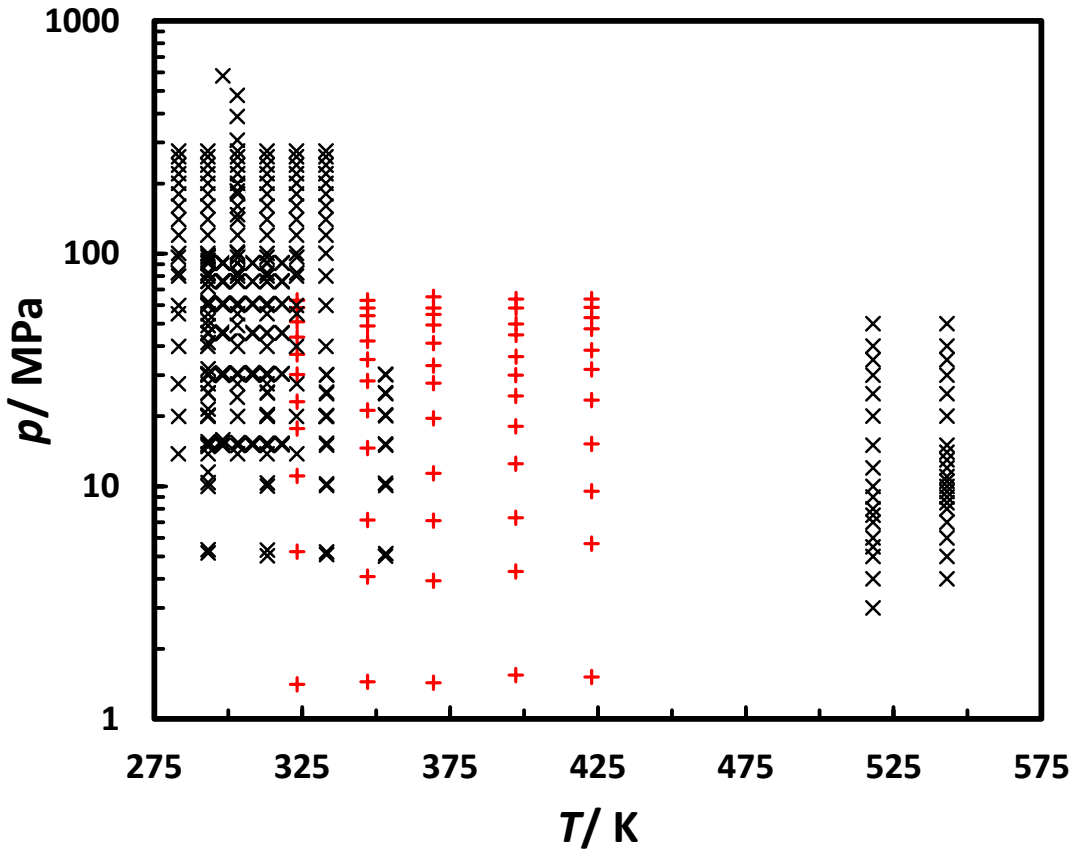

Figure 1. Distribution of the available experimental data for the speed of sound ***SoS*** in ethanol. (**×**): literature data (as tabulated in Table 2), (**+**): Measured in this work.

2. Material and Methods

2.1 Material

In this work nitrogen and water were used for calibration purposes. Details of the material used in this work including purity and supplier company, are tabulated in **Table 3**.

Table 3. Properties of the chemicals used in this study.

Chemical Name	CAS Number	Formula	Purity (mole%)	Supplier
Nitrogen	7727-37-9	N_2	99.99	BOC
Ethanol	46-17-5	C_2H_6O	>99.8	Fisher Scientific
Deionised water	7732-18-5	H_2O	100	PURELAB-DV25

2.2 Methods

2.2.1 Experimental setup

Simultaneous measurement of the density and the speed of sound were carried out using an acoustic cell and a vibrating tube densitometer. The densitometer and the acoustic cell were connected in parallel and housed in an oven as schematically depicted in **Figure 2**. Measurements were undertaken for five isotherms at (323.31, 347.10, 369.38, 397.28 and 422.90) K and pressures ranging up to 65 MPa. A detailed explanation of different parts of the setup can be found elsewhere. [45]

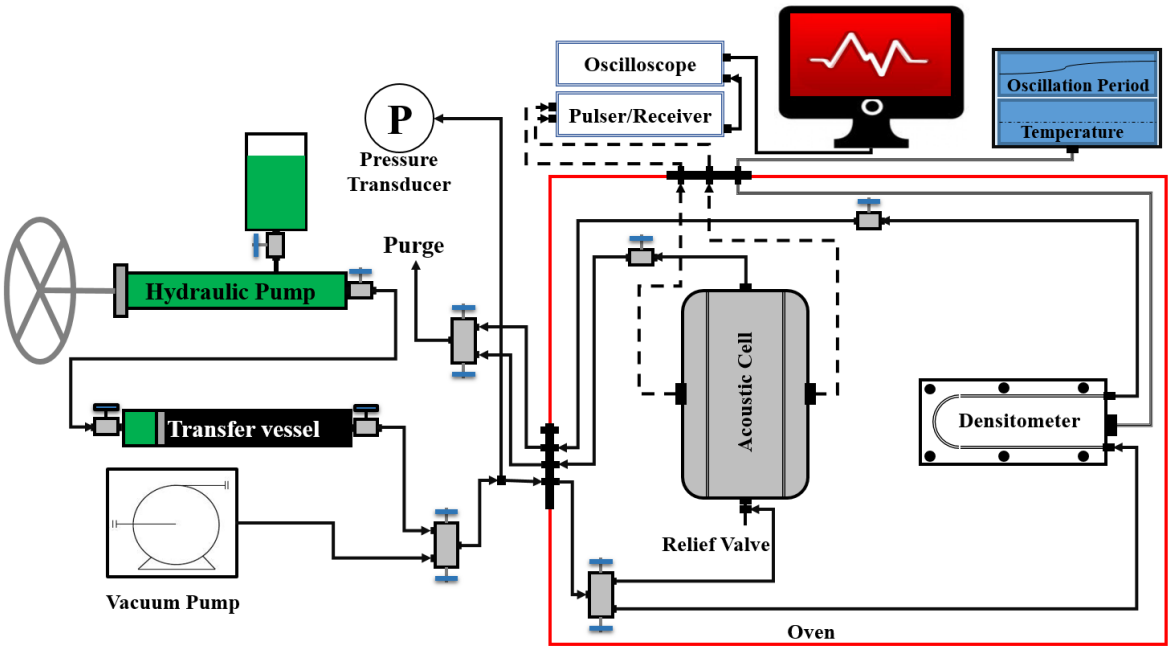

Figure 2. Schematic diagram of the system used to measure the density and the speed of sound simultaneously.

Densitometer: The HTHP U-shape vibrating tube densitometer (Anton Paar, model DMA HPM) used in this work can measure the density at temperatures between 263.15 K to 473.15 K and in a pressure range up to 140 MPa. The densitometer is equipped with a built-in temperature sensor (0.01K accuracy). Also, the temperature and pressure of the sample in the oven were set using an oven (Stuart Scientific, maximum working temperature: 523.15 K) and a hand pump (SITEC, maximum working pressure: 200 MPa), respectively. In this densitometer, the principle of the measurement is based on the measured oscillation period of the vibrating tube. The relation between oscillation period of the oscillator and the density of a fluid is calculated using the below equation:

$$\rho = C_1 \times \tau^2 + C_2 \qquad \text{eq. (1)}$$

where C_1 and C_2 are temperature and pressure dependent parameters of the oscillator and τ is the oscillation period of the oscillator. The oscillation period and sample temperature can be found quickly using an evaluation unit (Anton Paar, model mPDS5) connected to the densitometer. Moreover, the oscillator parameters were found by calibrating the densitometer against reference substances. This type of densitometer can provide precise results very quickly. However, the accuracy of the results is significantly dependent on the calibration procedure. The calibration procedure is discussed in details in the next section.

Acoustic cell: A cylindrical Inconel acoustic cell (internal volume ~130 ml) is utilised to measure the speed of sound in fluids. The apparatus is capable of working under HPHT condition up to 100 MPa and 523.15 K. However, due to the temperature limits of the ultrasonic transducers, the temperature of the acoustic cell should not exceed 448.15 K. To protect the acoustic cell against accidental overpressure, a pressure relief valve is connected to the cell. The ultrasonic transducers located on both sides of the cell were used to measure the sound velocity using the through-transmission method of ultrasonic testing. The transducers used in this setup are piezoelectric ultrasonic transceivers (X2002- delay line transducer, Frequency: 2-2.25 MHz). The transducers are fixed perpendicular to the surface of the acoustic cell and are aligned properly to prevent any misinterpretation of the signals. A pulsar-receiver (Panametrics, square wave-5077PR) is connected to the transducers to send and receive electrical signals. Also, an oscilloscope (Link Instruments, MSO 9201) is used to show the electrical signal in the form of a wave. The acoustic cell is schematically illustrated in **Figure 3**.

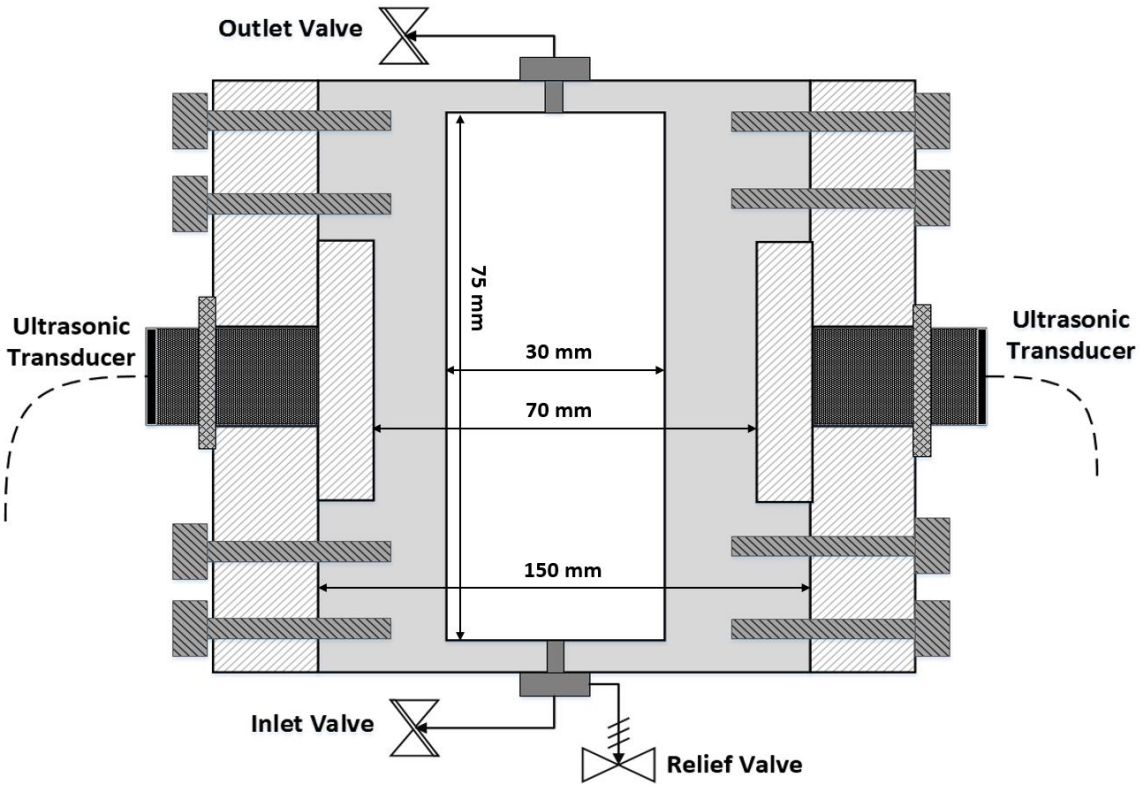

Figure 3. The schematic of the acoustic cell.

2.2.2 Setup calibration

Density measurement: as shown in eq. (1), to measure the density of a sample at any (*P*, *T*) of interest, knowledge of the oscillator parameters, C_1 and C_2, at the same (*P*, *T*) is required. Therefore, calibration tests were carried out to obtain the oscillation periods of two reference substances of well-known density values at the required range of pressure and temperature. Because of the reliable predictive tools available for obtaining the density of water and nitrogen over the (*P*, *T*) range of this work,these substances were used as reference components in this study. The density values of water and nitrogen were calculated employing IAPWS formulation for thermodynamic properties of water [46] and reference EoS for nitrogen [47]. Using the measured oscillation period of the sample and by replacing the calculated parameters of the oscillator, the final equation for determining the sample density can be expressed as:

$$\rho_S = (\tau_S^2 - \tau_{N_2}^2) \times \left[\frac{\rho_{H_2O} - \rho_{N_2}}{\tau_{H_2O}^2 - \tau_{N_2}^2}\right] + \rho_{N_2} \qquad \text{eq. (2)}$$

In this equation "s" denotes sample properties. Also, the properties of the reference substances (density and oscillation periods) were obtained at the same (*P*, *T*) condition of the sample.

The speed of sound measurement: To obtain the internal length of the acoustic cell at the required P-T range of this work, calibration tests were conducted using water as a reference. Employing the obtained reflection time at calibration test, and using the predicted values of the speed of sound in water from the IAPWS formulation for thermodynamic properties of water [46], the internal lengths of the acoustic cell were measured. The calibration tests were undertaken at same isotherms which experimental measurements needed to be conducted and in a pressure range up to 65 MPa. Therefore, at different pressures of each isotherm the reflection times were measured and the internal length was calculated. To simplify the estimation of the internal length at different pressures of each isotherm, the measured internal lengths were fitted to a linear function of pressure. Therefore, for each isotherm, a function was found to predict the internal length of the acoustic cell based on the system pressure.

The following calibration procedure was performed for both setups simultaneously at five isotherms and pressures ranging up to 65 MPa:

1. **System preparation:** The cleaned acoustic cell and the densitometer were filled with distilled water. The oven temperature was set to the desired temperature of the first isotherm and system was left for 24 hours to ensure temperature equilibrium in the system. Then, using the hand pump, water pressure in the acoustic cell was increased

to 65 MPa. Again the system was left for another 6 hours to reach thermodynamic equilibrium at the desired pressure and temperature.

2. **Conducting the measurements:** In the next step, measurement was conducted by running the oscilloscope to obtain the reflection time of sound waves. At the same time, the oscillation period of the oscillator was recorded. Then, system pressure was reduced by 2-3 MPa, and a new measurement was conducted. This procedure was repeated until pressure was reduced to 1-2 MPa. Finally, the oven temperature was changed to the next isotherm, and a similar procedure was repeated. Then, all the calibration procedures were repeated for the second reference substance in the densitometer. Lastly, the internal length of the acoustic cell and oscillation periods of the samples were found as a function of pressure at each isotherm.

2.2.3 Experimental measurements

The approach used to conduct the measurements was almost the same as the procedure used for calibration. Before conducting the measurements, the densitometer, the acoustic cells and connection lines were flushed with nitrogen and then vacuumed. Then, the oven temperature was set to the temperature of the first isotherm and ethanol was injected into the system and pressurised up to 5 MPa. After temperature stabilisation, the system pressure was increased up to 65 MPa. A few hours time was given to the system to ensure the stability of pressure and temperature in the system. Then, the first measurement was carried out by running the oscilloscope and measurement of the oscillation period and the reflection time. More measurements at the same temperature were performed by reducing the system pressure in 3-5 MPa steps. Finally, system temperature was set to the second isotherm, and similar measurements were carried out to obtain all required data.

2.2.4 Calculation of other derived properties

The approach used in this work to obtain derived properties of the fluid was based on the measured sound velocities and initial values of some properties (IVMs). In this technique, initial values of the density, speed of sound and isobaric heat capacity, as well as some thermodynamic relations, were used to obtain density and other derived properties of ethanol.

In the absence of absorption, the velocity of sound in a fluid (v) is related to the isentropic derivative of pressure with respect to the density (**eq. (3)**). [48] Employing the thermal expansivity coefficient (α_p), **eq. (3)** is simplified in the form of **eq. (4)**. Also, pressure derivative of the isobaric heat capacity for each isotherm is determined using **eq. (6)**. [49-50]

$$v^2 = \left(\frac{\partial p}{\partial \rho}\right)_s \quad \text{eq. (3)}$$

$$\alpha_p = -\frac{1}{\rho}\left(\frac{\partial \rho}{\partial T}\right)_p \quad \text{eq. (4)}$$

$$\left(\frac{\partial \rho}{\partial p}\right)_T = \frac{1}{v^2} + \frac{T}{C_p}{\alpha_p}^2 \quad \text{eq. (5)}$$

$$\left(\frac{\partial C_p}{\partial p}\right)_T = -\frac{T}{\rho}\left[{\alpha_p}^2 + \left(\frac{\partial \alpha_p}{\partial T}\right)_p\right] \quad \text{eq. (6)}$$

Lastly, using the procedure illustrated in **Figure 4**, the density and the isobaric heat capacity of ethanol were calculated for different temperatures at each pressure step. The ΔP shown in the figure is the pressure difference between two consecutive steps (P_{i+1} - P_i). Moreover, for ease of calculations, the estimated densities and thermal expansivities at each step were fitted to second-order polynomial functions of temperature. Using the polynomial functions the temperature derivatives of density and thermal expansion, $\left(\left(\frac{\partial \rho}{\partial T}\right)_p, \left(\frac{\partial \alpha_p}{\partial T}\right)_p\right)$, can be found easily. Furthermore, the isochoric heat capacity (C_v) and the Joule-Thomson coefficient were calculated according to the following equations;

$$\beta_T = -\frac{1}{\rho}\left(\frac{\partial \rho}{\partial P}\right)_T \quad \text{eq. (7)}$$

$$\beta_s = \frac{1}{\rho v^2} \quad \text{eq. (8)}$$

$$C_v = C_p \frac{\beta_s}{\beta_T} \quad \text{eq. (9)}$$

$$\mu_{JT} = \frac{T\alpha_p - 1}{\rho C_p} \quad \text{eq. (10)}$$

In the above equations, β_T, β_S and μ_{JT} stand for isothermal compressibility, isentropic compressibility and Joule-Thomson coefficient, respecitvely.

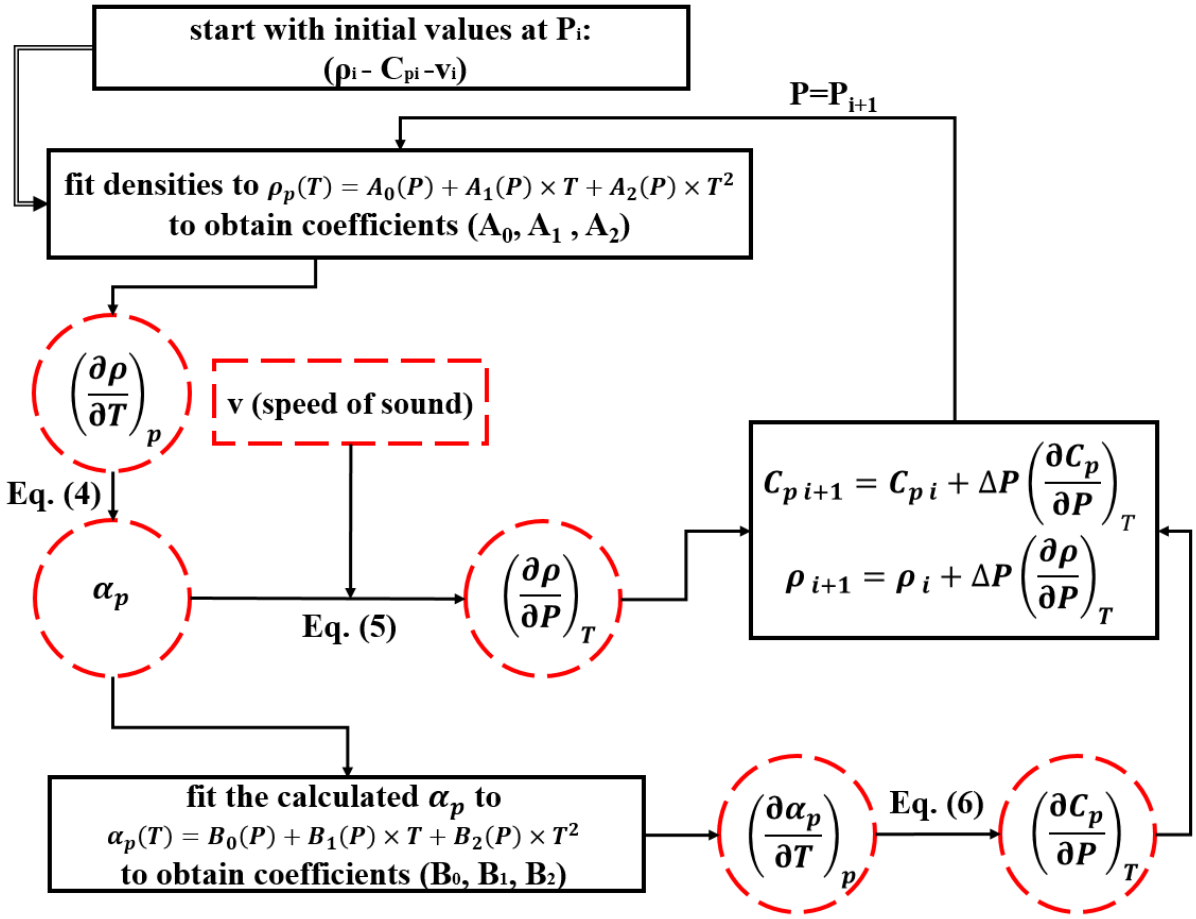

Figure 4. Schematic flowchart for calculation of density and isobaric heat capacity of the fluid.

For the method used in this work, the initial values of the isobaric heat capacity, density and sound velocity were estimated using the predictive model of Schroeder et al. [6] Also, values of the speed of sound at any (*P*, *T*) of interest were estimated using a model fitted to the measured sound velocities. This model was developed using a machine learning approach to firstly fit a model in the range of observation data, and secondly to predict the response with associated uncertainty. In this work, a flexible prior was placed on functions that do not belong to any parametric family. To do so, a Gaussian Process Regression (GPR) model was introduced as a well-founded framework for non-parametric model selection. A GPR can take the form of a full predictive distribution at any instance of input variables (e.g. temperature and pressure), provided that a mean function and a positive-definite kernel are known. [51-52] The parameters of the GPR model were initially inferred through the training phase, cross-validated to avoid overfitting in the validation phase, and finally tested on a set of unseen data to quantify the predictive performance of the model.

3. Result and discussion

3.1 Density and the speed of sound

The simultaneously measured densities and the speed of sound (*SoS*) in ethanol for five isotherms of (323.31, 347.10, 369.38, 397.28 and 422.90) K and pressures ranging up to 65 MPa, are tabulated in **Table 4** to **Table 8**. The measured properties were then compared against predictions of the Schroeder et al. - EoS [6]. The reported deviations were calculated according to the equation below:

$$Deviation(\%) = 100 \times \frac{(X^{Exp} - X^{EoS})}{X^{Exp}} \qquad \text{eq. (11)}$$

Also, the expanded uncertainty (with 95 % level of confidence, k=2) of the measurements were calculated employing the procedure illustrated in **APPENDIX**. The overall average expanded uncertainty (k=2) of the measured densities and the sound velocities were calculated to be 0.05 % and 0.11 %, respectively.

Table 4. Measured densities ρ and sound velocities *SoS* in ethanol at *T*= (323.31±0.02) K. [a]

P MPa	Exp *SoS* (m.s^{-1})	Uncertainty (m.s^{-1})	Deviation (%)	Exp ρ (mol.m^{-3})	Uncertainty (mol.m^{-3})	Deviation (%)
1.410	1070.65	1.15	0.16	16594	7	0.00
5.245	1096.75	1.19	0.03	16680	7	0.01
11.101	1135.02	1.25	-0.02	16800	7	0.01
17.687	1174.47	1.31	-0.06	16927	7	0.00
23.114	1204.23	1.36	-0.13	17029	7	0.03
30.237	1241.91	1.43	-0.1	17152	7	0.04
36.831	1274.55	1.49	-0.08	17261	7	0.05
43.809	1306.05	1.55	-0.14	17370	7	0.07
50.864	1337.26	1.61	-0.12	17473	7	0.06
58.500	1369.40	1.67	-0.09	17579	7	0.07
62.862	1386.24	1.70	-0.14	17641	7	0.09
	% AAD		**0.10**			**0.04**

[a] In comparison with predictions of the Schroeder et al. - EoS [6]. Expanded uncertainties of the measured densities reported with 95 % level of confidence. Expanded uncertainties of all the measured pressures (with 95 % level of confidence)=0.036 MPa.

Table 5. Measured densities ρ and sound velocities *SoS* in ethanol at T = (347.10±0.03) K. [a]

P MPa	Exp *SoS* ($m.s^{-1}$)	Uncertainty[a] ($m.s^{-1}$)	Deviation (%)	Exp ρ ($mol.m^{-3}$)	Uncertainty[a] ($mol.m^{-3}$)	Deviation (%)
1.446	991.29	1.04	-0.19	16116	8	0.00
4.092	1011.79	1.07	-0.19	16185	8	0.01
7.163	1035.01	1.10	-0.29	16261	8	0.01
14.616	1085.64	1.17	-0.30	16432	8	0.00
21.177	1126.37	1.23	-0.27	16570	8	0.00
28.408	1168.14	1.30	-0.26	16711	8	0.01
35.022	1203.39	1.36	-0.25	16833	8	0.01
42.067	1238.63	1.42	-0.25	16954	8	0.01
48.843	1270.33	1.48	-0.24	17065	8	0.02
54.137	1294.14	1.52	-0.22	17148	8	0.03
58.348	1312.64	1.56	-0.22	17213	8	0.04
62.859	1331.57	1.59	-0.19	17285	7	0.08
	% AAD		**0.23**			**0.02**

[a] In comparison with predictions of the Schroeder et al. - EoS [6]. Expanded uncertainties of the measured densities reported with 95 % level of confidence. Expanded uncertainties of all the measured pressures (with 95 % level of confidence)=0.036 MPa.

Table 6. Measured densities ρ and sound velocities *SoS* in ethanol at T =(369.38±0.02) K. [a]

P MPa	Exp *SoS* ($m.s^{-1}$)	Uncertainty[a] ($m.s^{-1}$)	Deviation (%)	Exp ρ ($mol.m^{-3}$)	Uncertainty[a] ($mol.m^{-3}$)	Deviation (%)
1.432	914.53	0.95	-0.29	15614	8	-0.09
3.923	936.50	0.97	-0.34	15691	8	-0.08
7.109	963.26	1.00	-0.35	15784	8	-0.08
11.382	996.24	1.04	-0.40	15901	8	-0.07
19.601	1053.82	1.12	-0.42	16107	7	-0.05
27.704	1104.72	1.20	-0.39	16289	7	-0.04
33.060	1135.35	1.24	-0.4	16399	7	-0.04
41.165	1179.11	1.32	-0.36	16556	7	-0.03
49.42	1220.33	1.39	-0.33	16705	7	-0.01
54.796	1246.14	1.43	-0.28	16795	7	-0.02
58.367	1261.46	1.46	-0.35	16852	7	-0.02
65.148	1291.23	1.51	-0.34	16953	7	-0.06
	% AAD		**0.35**			**0.05**

[a] In comparison with predictions of the Schroeder et al. - EoS [6]. Expanded uncertainties of the measured densities reported with 95 % level of confidence. Expanded uncertainties of all the measured pressures (with 95 % level of confidence)=0.036 MPa.

Table 7. Measured densities ρ and sound velocities *SoS* in ethanol at T =(397.28±0.02)K. [a]

P MPa	Exp *SoS* (m.s^{-1})	Uncertainty (*k*=2) (m.s^{-1})	Deviation (%)	Exp ρ (mol.m^{-3})	Uncertainty (*k*=2) (mol.m^{-3})	Deviation (%)
1.546	811.26	0.85	-0.31	14904	8	-0.13
4.302	840.39	0.87	-0.39	15012	8	-0.14
7.333	870.18	0.90	-0.43	15126	8	-0.13
12.482	915.79	0.94	-0.50	15301	8	-0.12
18.105	960.62	0.99	-0.52	15473	8	-0.10
24.432	1006.22	1.05	-0.51	15648	8	-0.09
29.996	1043.31	1.10	-0.47	15790	7	-0.07
36.074	1080.66	1.16	-0.44	15933	7	-0.06
44.752	1129.46	1.23	-0.44	16122	7	-0.04
49.805	1156.02	1.27	-0.43	16224	7	-0.03
58.415	1198.58	1.35	-0.42	16387	7	-0.02
63.790	1223.51	1.39	-0.44	16485	7	0.00
	% AAD		**0.44**			**0.09**

[a] In comparison with predictions of the Schroeder et al. - EoS [6]. Expanded uncertainties of the measured densities reported with 95 % level of confidence. Expanded uncertainties of all the measured pressures (with 95 % level of confidence)=0.036 MPa.

Table 8. Measured densities ρ and sound velocities *SoS* in ethanol at T =(422.90±0.01)K. [a]

P MPa	Exp SoS (m.s^{-1})	Uncertainty (m.s^{-1})	Deviation (%)	Exp ρ (mol.m^{-3})	Uncertainty (mol.m^{-3})	Deviation (%)
1.514	701.53	0.80	0.02	14119	8	-0.13
5.675	755.36	0.81	-0.20	14342	8	-0.13
9.530	798.44	0.83	-0.34	14521	8	-0.13
15.206	853.77	0.87	-0.47	14754	8	-0.11
23.492	923.37	0.94	-0.52	15043	8	-0.09
31.793	984.06	1.02	-0.48	15291	8	-0.08
38.446	1027.65	1.08	-0.45	15469	8	-0.07
47.571	1081.97	1.16	-0.42	15690	7	-0.06
53.132	1112.23	1.20	-0.44	15816	7	-0.04
58.734	1141.24	1.25	-0.44	15933	7	-0.03
63.754	1166.21	1.29	-0.44	16029	7	-0.06

% AAD	**0.38**		**0.08**

[a] In comparison with predictions of the Schroeder et al. - EoS [6]. Expanded uncertainties of the measured densities reported with 95 % level of confidence. Expanded uncertainties of all the measured pressures (with 95 % level of confidence)=0.036 MPa.

The measured and predicted density of ethanol are depicted in **Figure 5**. Also, deviations of the measured densities in comparison with the model are shown in **Figure 6**. As shown in this figure, for all the measured densities the observed deviations were less than 0.15 % which lie within the uncertainty of the model used in this work (u_ρ= ±0.2 %). Also, the overall average absolute deviation (% AAD) of the experimental results in comparison with the model predictions were found to be 0.05 % indicating a reasonable agreement between measured and predicted densities. The following equation was used to caluclated % AAD of the measured properties in comparison with predictions of the model:

$$\% AAD = 100 \times \frac{\sum_i^N \frac{\left|X_i^{Exp} - X_i^{EoS}\right|}{X_i^{Exp}}}{N} \qquad \text{eq. (12)}$$

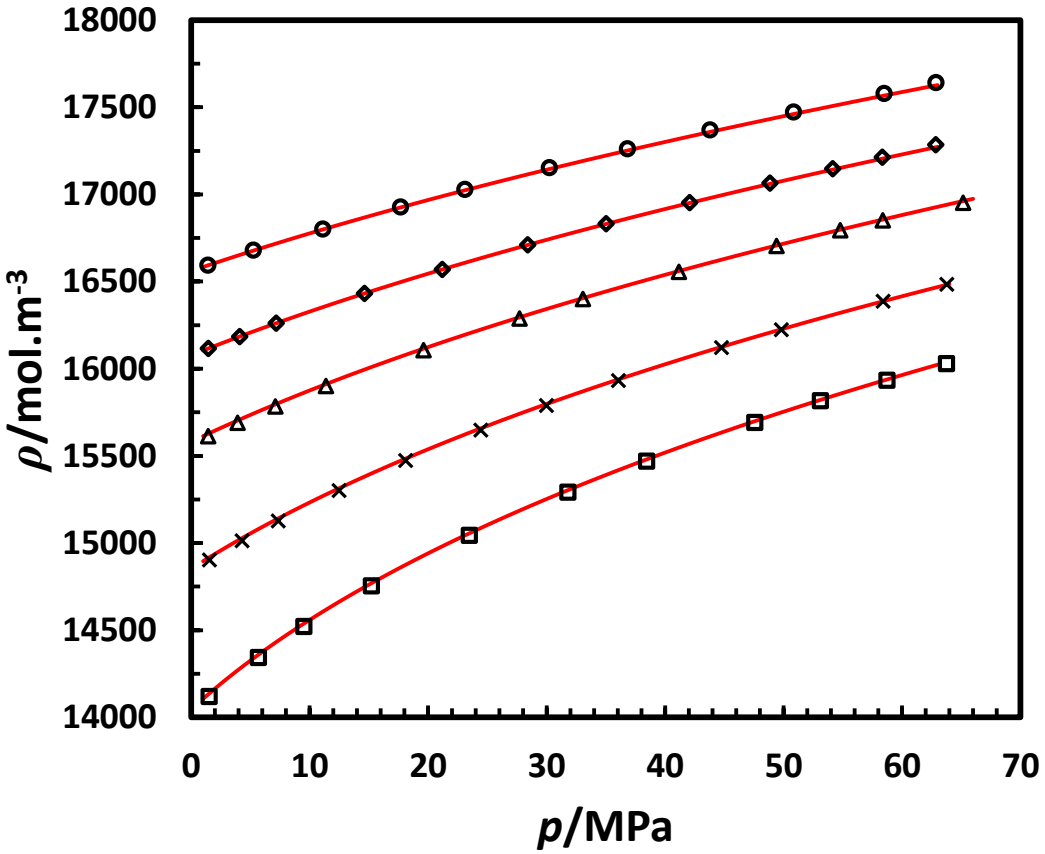

Figure 5. Measured and predicted densities ρ of ethanol for different isotherms. (○): 323.27 K, (◊):347.01 K, (Δ):369.45 K, (×):397.28 K, (□):422.90 K, (—): predictions of the Schroeder et al.-EoS.

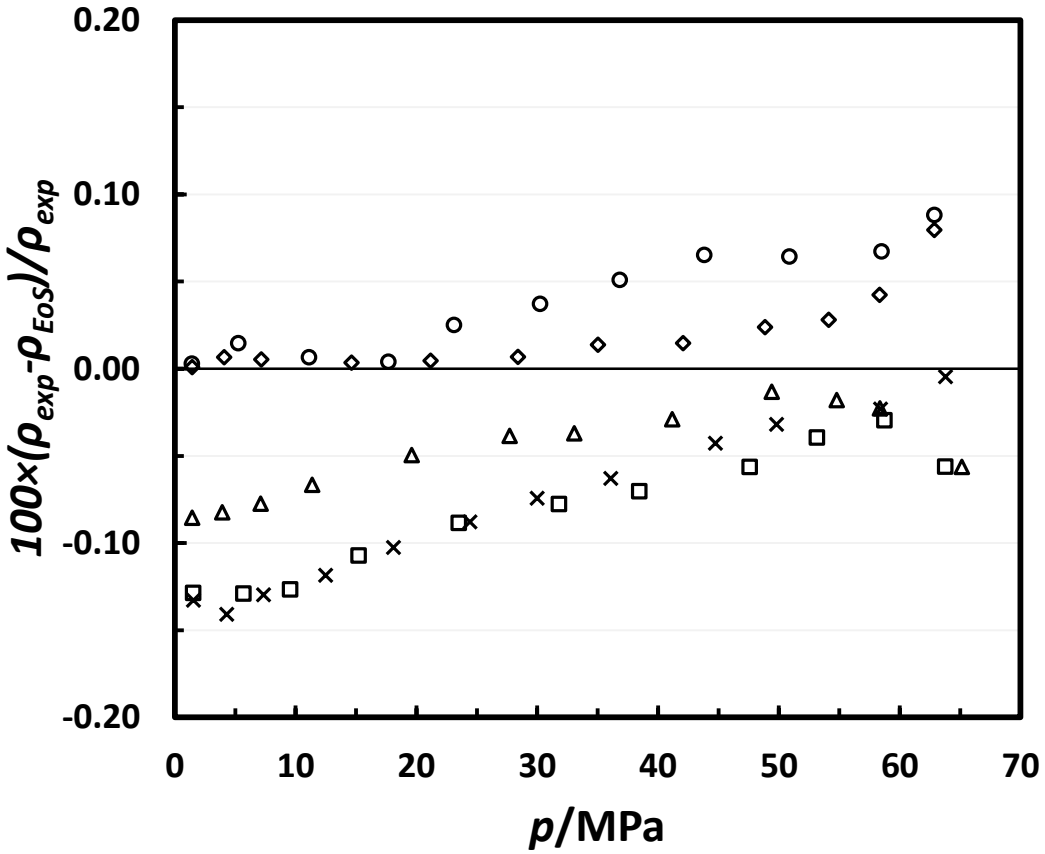

Figure 6. Deviations of the measured densities ρ in comparison with the predictions of Schroeder et al. – EoS [6]. (○): 323.27 K, (◊):347.01 K, (Δ):369.45 K, (×):397.28 K, (□):422.90 K.

The measured sound velocities of this work, predictions of the model, and a few data points measured and reported in the literature are shown in **Figure 7**. The literature data shown in this graph were measured at temperatures slightly different from the first isotherm of this work. The % AAD of the results in comparison to the predictive model [6], was found to be 0.30 %. As depicted in **Figure 8**, the observed deviation in some points increased up to 0.52 % which is less than the reported uncertainty of the model (u_v = ±1.0 %). However, analysis of the measured sound velocities in ethanol from different references in the literature indicates similar deviations when experimental results were compared to the model used in this work. For instance, the % AAD of the model in comparison to the results obtained by Sun et al. [9], Wilson and Bradley [43] and Wegge et al. [7], were found to be 0.24 %, 0.15 % and 0.30 %, respectively.

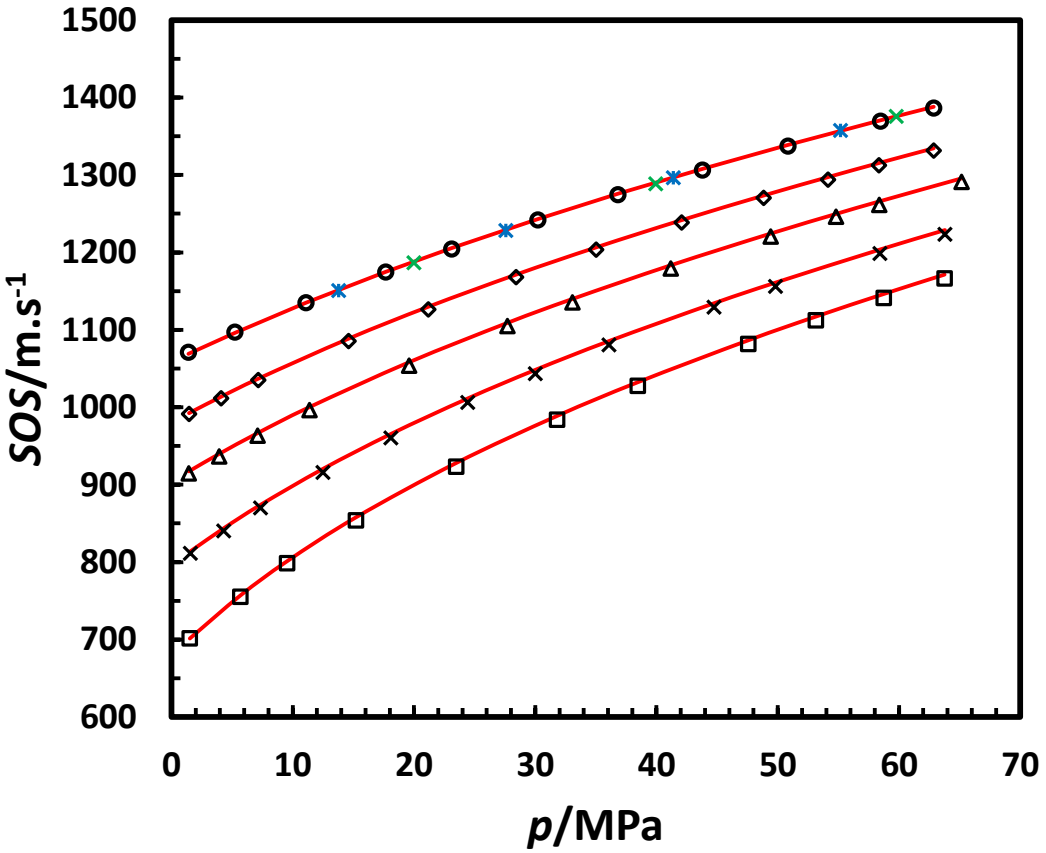

Figure 7. Comparison of the measured sound velocities *SoS*, model predictions and available literature data at different isotherms. (○): 323.27 K, (◊):347.01 K, (Δ):369.45 K, (×):397.28 K, (□):422.90 K. (—): predictions of the Schroeder et al.-EoS; (×): Measured sound velocities at 323.02 K.[9]; (Ж): Measured sound velocities at 323.15 K.[43]

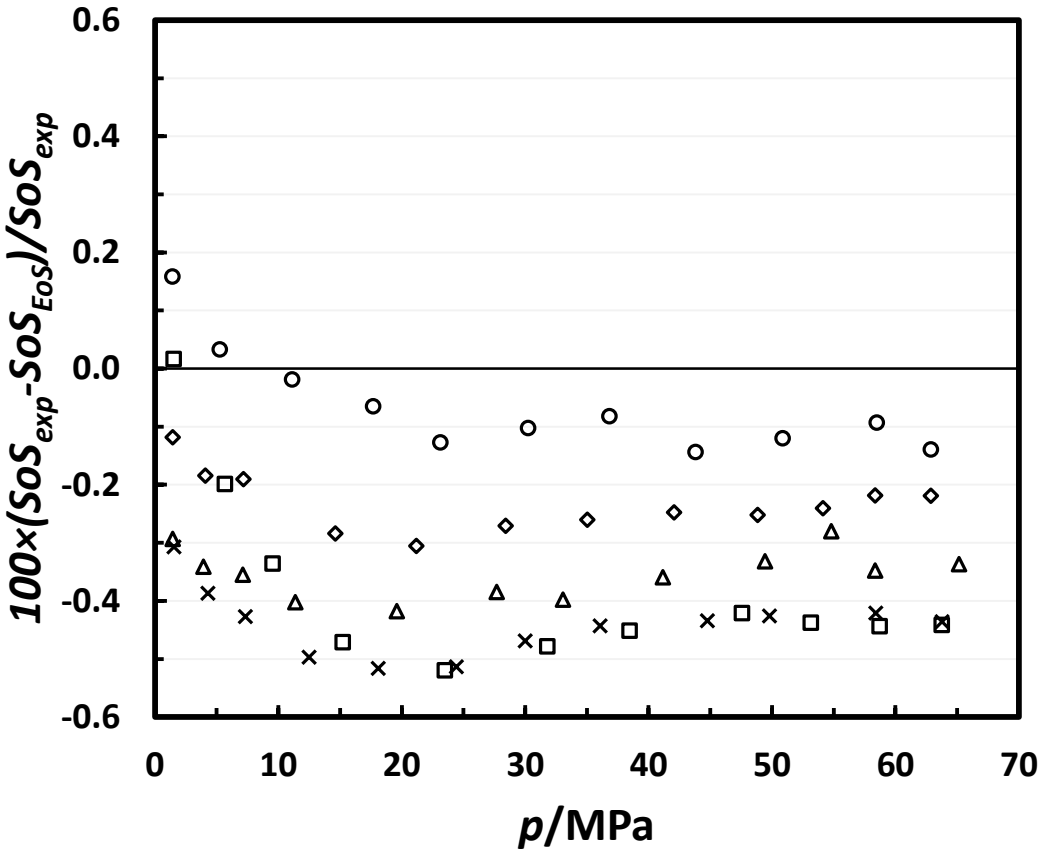

Figure 8. Deviations of the measured sound velocities *SoS* in comparison with the predictions of Schroeder et al. – EoS. (○): 323.27 K, (◊):347.01 K, (Δ):369.45 K, (×):397.28 K, (□):422.90 K. The uncertainty of the equation of state is ±1.0 %.

3.2 Derived properties

As mentioned before, based on the measured sound velocities a GPR model was developed to predict the speed of sound at any (*P*, *T*) of interest. To check the GPR model, the measured sound velocities and predictions of the GPR model are tabulated in **Table 9**. The % AAD of the predicted sound velocities of the GPR model in comparison to the measured values was found to be 0.05%. Also, further investigation was conducted to check the validity of the GPR model. In this way, some literature data measured at (*P*, *T*) ranges within the (*P*, *T*) range of this work were compared to predictions of the GPR model. As shown in **Table 10**, the % AAD between predictions of the GPR model and measured sound velocities of different sources in the literature was calculated to be 0.17 %.

Using the procedure illustrated in **Figure 4,** and employing the predicted sound velocities from the GPR model, density, isobaric and isochoric heat capacities and Joule-Thomson coefficient can be calculated.

Table 9. Comparison of the measured sound velocities *SoS* and predictions of the *GPR* model used in this work.[a]

T	*P*	Exp. *SoS*	Uncertainty	Predicted *SoS*	Uncertainty	Deviation (%)
K	MPa	($m.s^{-1}$)	($m.s^{-1}$)	($m.s^{-1}$)	($m.s^{-1}$)	
323.32	62.862	1386.24	1.44	1385.83	2.07	0.03
323.32	58.500	1369.40	1.41	1369.18	1.88	0.02
323.32	50.864	1337.26	1.35	1337.81	1.84	-0.04
323.31	43.809	1306.05	1.29	1306.72	1.84	-0.05
323.31	36.831	1274.55	1.23	1274.14	1.82	0.03
323.31	30.237	1241.91	1.17	1241.64	1.81	0.02
323.30	23.114	1204.23	1.11	1204.38	1.82	-0.01
323.29	17.687	1174.47	1.06	1174.17	1.83	0.03
323.30	11.101	1135.02	1.00	1134.82	1.83	0.02
323.31	5.245	1096.75	0.95	1096.94	1.87	-0.02
323.30	1.410	1070.65	0.91	1070.48	2.05	0.02
347.07	62.859	1331.57	1.33	1331.87	1.89	-0.02
347.07	58.348	1312.64	1.30	1312.87	1.79	-0.02
347.07	54.137	1294.14	1.26	1294.43	1.77	-0.02
347.07	48.843	1270.33	1.22	1270.38	1.77	0.00
347.07	42.067	1238.63	1.17	1238.25	1.76	0.03
347.10	35.022	1203.39	1.11	1203.01	1.75	0.03
347.11	28.408	1168.14	1.05	1167.98	1.76	0.01
347.11	21.177	1126.37	0.99	1126.84	1.76	-0.04
347.12	14.616	1085.64	0.93	1086.13	1.77	-0.04
347.13	7.163	1035.01	0.86	1034.98	1.77	0.00
347.14	4.092	1011.79	0.83	1012.10	1.79	-0.03
347.14	1.446	991.29	0.81	991.48	1.87	-0.02
369.36	65.148	1291.23	1.26	1291.79	1.96	-0.04
369.37	58.367	1261.46	1.20	1261.60	1.77	-0.01
369.37	54.796	1246.14	1.18	1245.13	1.76	0.08
369.37	49.420	1220.33	1.13	1219.61	1.75	0.06
369.37	41.165	1179.11	1.07	1178.55	1.75	0.05
369.37	33.060	1135.35	1.00	1135.43	1.76	-0.01
369.38	27.704	1104.72	0.95	1104.84	1.75	-0.01
369.38	19.601	1053.82	0.88	1054.36	1.75	-0.05
369.38	11.382	996.24	0.81	996.38	1.75	-0.01
369.38	7.109	963.26	0.78	962.91	1.75	0.04
369.38	3.923	936.50	0.75	936.26	1.77	0.03
369.38	1.432	914.53	0.73	914.34	1.84	0.02
397.31	63.790	1223.51	1.14	1223.88	1.95	-0.03

T K	*P* MPa	Exp. *SoS* (m.s^{-1})	Uncertainty (m.s^{-1})	Predicted *SoS* (m.s^{-1})	Uncertainty (m.s^{-1})	Deviation (%)
397.31	58.415	1198.58	1.09	1198.32	1.83	0.02
397.30	49.805	1156.02	1.03	1155.60	1.80	0.04
397.29	44.752	1129.46	0.98	1129.29	1.78	0.02
397.28	36.074	1080.66	0.91	1081.05	1.76	-0.04
397.27	29.996	1043.31	0.86	1044.16	1.76	-0.08
397.27	24.432	1006.22	0.82	1007.38	1.76	-0.12
397.27	18.105	960.62	0.77	961.20	1.77	-0.06
397.26	12.482	915.79	0.72	915.53	1.77	0.03
397.26	7.333	870.18	0.69	869.18	1.77	0.11
397.26	4.302	840.39	0.67	839.68	1.80	0.08
397.25	1.546	811.28	0.66	811.37	1.89	-0.01
422.92	63.754	1166.21	1.04	1166.19	2.09	0.00
422.92	58.734	1141.24	1.00	1141.05	1.86	0.02
422.90	53.132	1112.23	0.96	1112.03	1.83	0.02
422.90	47.571	1081.97	0.91	1081.84	1.84	0.01
422.90	38.446	1027.65	0.84	1028.31	1.84	-0.06
422.90	31.793	984.06	0.79	984.90	1.83	-0.09
422.89	23.492	923.37	0.72	923.63	1.84	-0.03
422.89	15.206	853.77	0.67	852.21	1.84	0.18
422.89	9.530	798.44	0.64	796.09	1.82	0.29
422.89	5.675	755.36	0.64	754.20	1.85	0.15
422.89	1.514	701.53	0.65	705.28	2.05	-0.53
					% AAD	**0.05**

[a] level of confidence for uncertainties=0.95, (k =2). $Deviation\ (\%) = 100 \times \frac{(X^{EXP} - X^{GPR})}{X^{EXP}}$.

Table 10. Comparison of the experimental results from different references in the literature with predictions of the *GPR* model used in this work.

T / K	P / MPa	Measured SoS / (m.s^{-1})	Predicted SoS / (m.s^{-1})	$100 \times \frac{(SoS_{EXP} - SoS_{Predicted})}{SoS_{EXP}}$
323.02	19.990	1186.60 [9]	1187.99	-0.12
323.02	39.930	1288.50 [9]	1289.59	-0.08
323.02	59.770	1375.80 [9]	1374.83	0.07
333.01	19.990	1158.10 [9]	1159.53	-0.12
333.01	39.930	1263.30 [9]	1263.65	-0.03
333.01	59.770	1352.50 [9]	1351.54	0.07
323.15	13.790	1150.91 [43]	1151.70	-0.07
323.15	27.579	1228.43 [43]	1228.45	0.00
323.15	55.158	1357.38 [43]	1356.18	0.09
333.21	30.214	1212.32 [7]	1214.75	-0.20
333.21	25.377	1186.40 [7]	1189.09	-0.23
333.21	20.181	1157.08 [7]	1160.07	-0.26
333.21	15.294	1127.88 [7]	1131.15	-0.29
333.21	10.228	1095.91 [7]	1099.19	-0.30
333.21	5.213	1062.10 [7]	1065.25	-0.30
353.21	30.289	1160.47 [7]	1162.13	-0.14
353.21	25.250	1131.76 [7]	1133.91	-0.19
353.21	20.273	1101.73 [7]	1104.33	-0.24
353.21	15.211	1069.36 [7]	1072.16	-0.26
353.21	10.319	1035.89 [7]	1038.69	-0.27
353.21	5.006	996.76 [7]	999.28	-0.25
			% AAD	**0.17**

Comparison of the calculated and measured densities in this work and predictions of the Schroeder et al.-EoS are depicted in **Figure 9**. Also, the calculated isobaric and isochoric heat capacities and Joule-Thomson coefficients of ethanol are shown in **Figure 10** to **Figure 12** respectively. Furthermore, numerical values of the density, isobaric and isochoric heat capacities and Joule-Thomson coefficients and deviations of the estimated properties in comparison with predictions of the Schroeder et al.-EoS are tabulated in **Table 11** to **Table 14**. In these tables following equation was used to calculate deviations:

$$Deviation\ (\%) = 100 \times \frac{(X^{calculated} - X^{EoS})}{X^{Calculated}} \qquad \text{eq. (13)}$$

As shown in **Figure 9**, a reasonable agreement was observed between measured densities and calculated values. However, as shown in **Table 11**, the deviations of the calculated densities in comparison to predictions of the model increase at higher temperatures.

For the estimated isobaric heat capacities and Joule-Thomson coefficient, the most significant deviations were observed at two isotherms of 369.38 K and 422.90 K. Also, for the isochoric heat capacity, largest deviations were observed for the isotherm with the highest temperature (422.90 K). As shown in **Table 9**, the maximum deviations of the predicted velocities in comparison to the measured values were observed at the isotherm with highest temperature. Therefore, larger deviations of the derived properties from the Schroeder et al.-EoS was expected at this isotherm. The obtained heat capacities are within the range of the uncertainties of the Schroeder et al.- EoS[6]. As reported by Schroeder et al., deviations between experimental isobaric heat capacity data and predictions, in the investigated temperature and pressure range of this study, are typically 5% or greater. This value is much larger than the observed deviations in this study

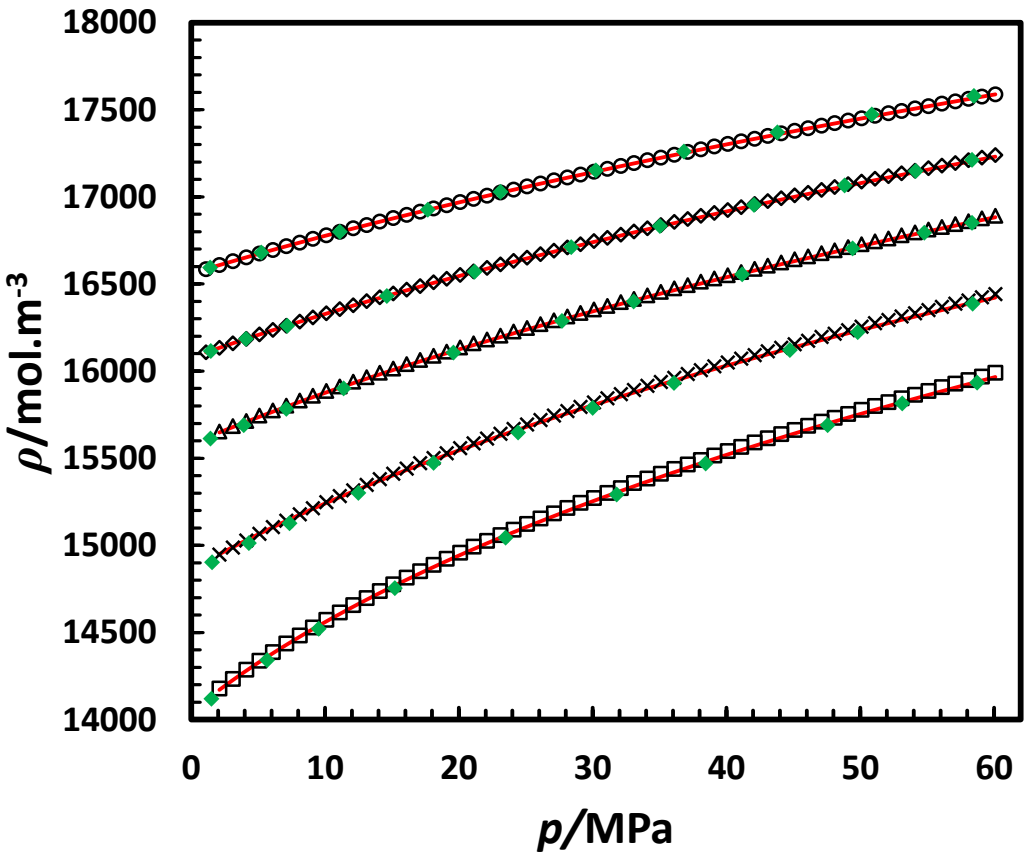

Figure 9. Comparison of the densities ρ calculated using initial value method and the EoS of Schroeder et al. with experimental results. (○): 323.27 K, (◊):347.01 K, (Δ):369.45 K, (×):397.28 K, (□):422.90 K, (—): predictions of the Schroeder et al.-EoS, (♦): experimental results of this work.

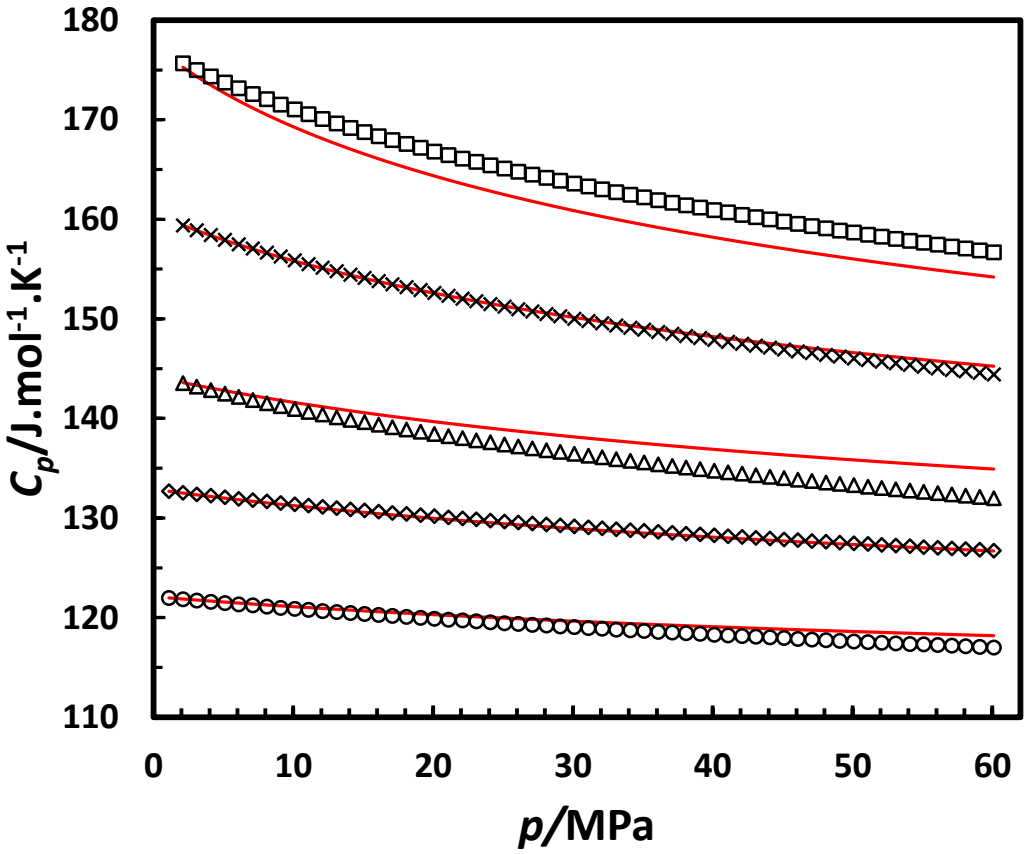

Figure 10. Comparison of the isobaric heat capacities C_p calculated using initial value method and Schroeder et al.-EoS. (○): 323.27 K, (◊):347.01 K, (Δ):369.45 K, (×):397.28 K, (□):422.90 K, (—): predictions of the Schroeder et al.-EoS.

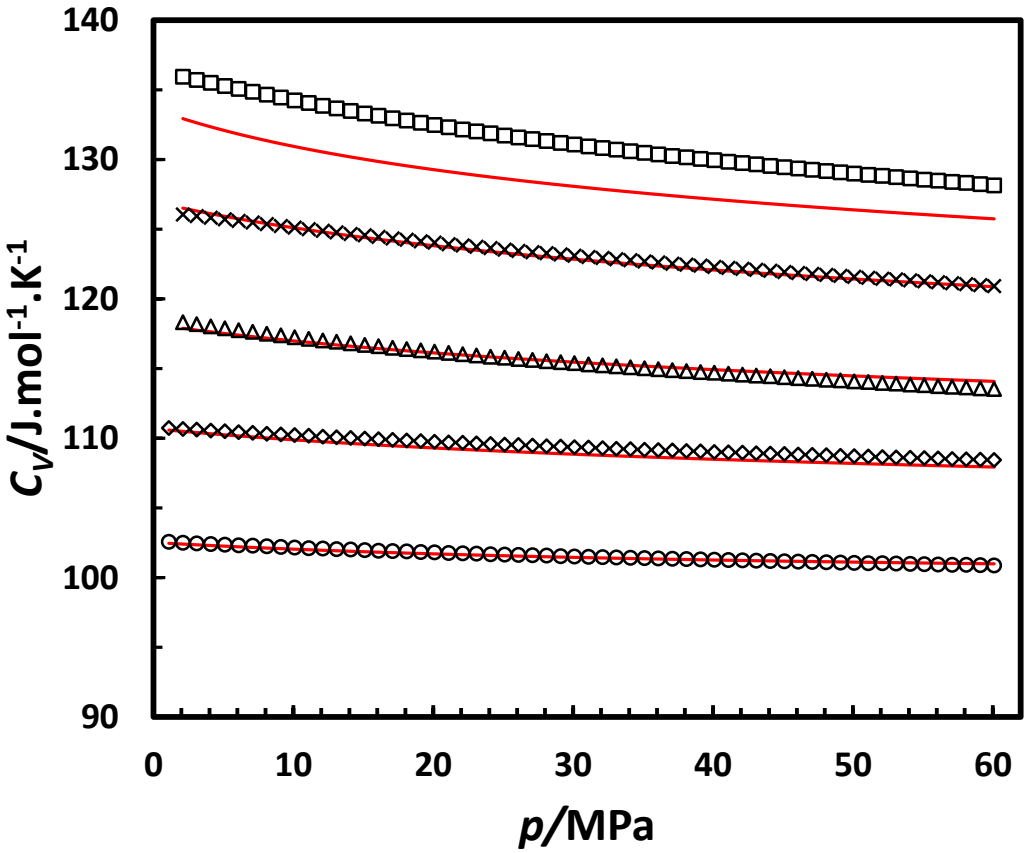

Figure 11. Comparison of the isochoric heat capacities C_v calculated using initial value method and the EoS of Schroeder et al. (○): 323.27 K, (◊):347.01 K, (Δ):369.45 K, (×):397.28 K, (□):422.90 K, (—): predictions of the Schroeder et al.-EoS.

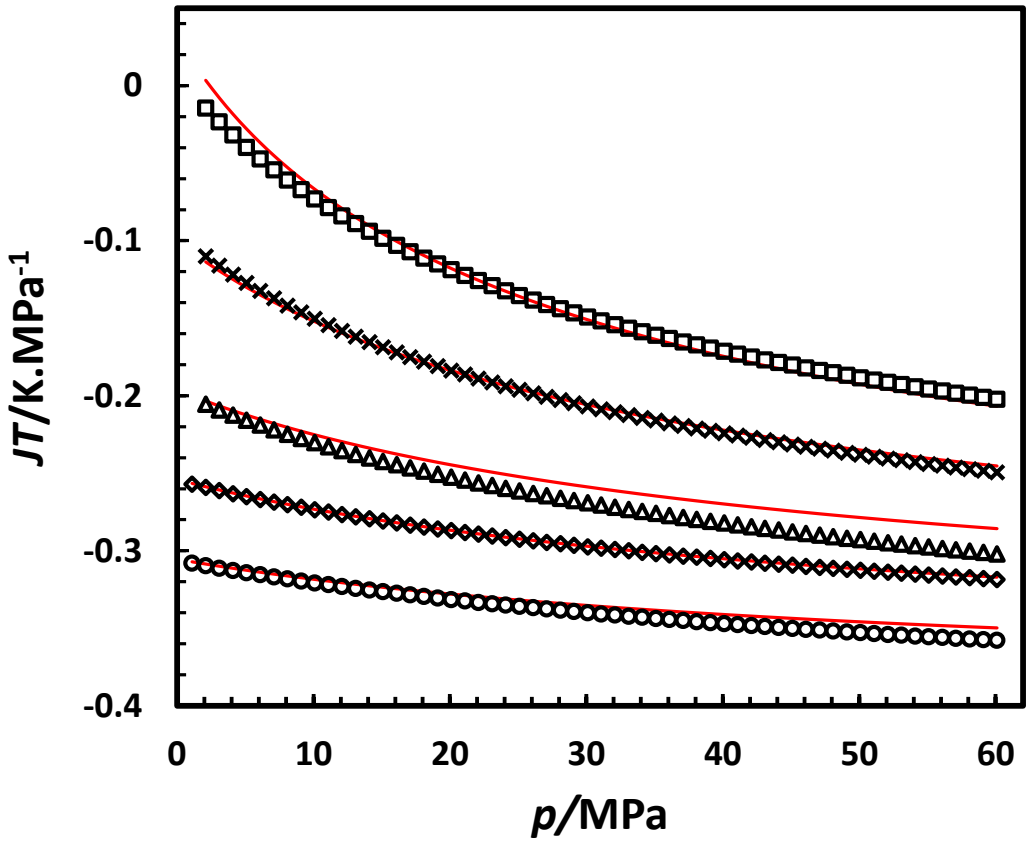

Figure 12. Comparison of the calculated Joule-Thomson coefficients *JT* using initial value method with predictions of the Schroeder et al.-EoS. (○): 323.27 K, (◊):347.01 K, (Δ):369.45 K, (×):397.28 K, (□):422.90 K, (—): predictions of the Schroeder et al.-EoS.

Table 11. Calculated densities ρ (mol.m^{-3}) of ethanol at different isotherms.

P/MPa	*T*=323.31 K	Deviation (%)	*T*=347.10 K	Deviation (%)	*T*=369.38 K	Deviation (%)	*T*=397.28 K	Deviation (%)	*T*=422.90 K	Deviation (%)
5.1	16675	0.00	16211	0.01	15744	0.04	15067	0.00	14338	0.05
10.1	16779	0.00	16333	0.01	15886	0.05	15248	0.03	14573	0.06
15.1	16878	0.01	16446	0.02	16015	0.05	15410	0.05	14777	0.08
20.1	16971	0.01	16552	0.03	16136	0.06	15558	0.07	14958	0.09
25.1	17060	0.01	16652	0.03	16249	0.06	15694	0.08	15122	0.10
30.1	17145	0.01	16747	0.03	16355	0.06	15820	0.09	15272	0.11
35.1	17226	0.01	16838	0.04	16455	0.06	15938	0.09	15411	0.12
40.1	17304	0.01	16925	0.04	16550	0.06	16049	0.10	15541	0.12
45.1	17379	0.01	17008	0.04	16641	0.06	16155	0.10	15663	0.13
50.1	17452	0.01	17088	0.05	16728	0.06	16255	0.11	15777	0.14
55.1	17522	0.01	17165	0.05	16812	0.05	16350	0.11	15886	0.14
60.1	17590	0.00	17239	0.05	16892	0.05	16442	0.12	15990	0.15

Table 12. Calculated isobaric heat capacities C_p (J.mol^{-1}.K^{-1}) of ethanol at different isotherms.

P/MPa	*T*=323.31 K	Deviation (%)	*T*=347.10 K	Deviation (%)	*T*=369.38 K	Deviation (%)	*T*=397.28 K	Deviation (%)	*T*=422.90 K	Deviation (%)
5.1	121.45	-0.09	132.08	0.07	142.48	-0.21	157.94	0.03	173.74	0.63
10.1	120.88	-0.17	131.38	0.11	140.94	-0.47	155.87	0.05	171.03	1.05
15.1	120.36	-0.26	130.76	0.15	139.62	-0.69	154.12	0.04	168.76	1.31
20.1	119.89	-0.34	130.18	0.16	138.45	-0.89	152.59	0.01	166.81	1.48
25.1	119.45	-0.42	129.65	0.17	137.40	-1.07	151.23	-0.03	165.10	1.59
30.1	119.04	-0.50	129.16	0.17	136.45	-1.25	150.01	-0.08	163.57	1.66
35.1	118.65	-0.59	128.70	0.16	135.57	-1.42	148.90	-0.15	162.19	1.69
40.1	118.29	-0.67	128.26	0.15	134.76	-1.58	147.88	-0.22	160.92	1.70
45.1	117.94	-0.76	127.85	0.13	134.00	-1.75	146.93	-0.30	159.75	1.70
50.1	117.61	-0.84	127.46	0.10	133.29	-1.91	146.04	-0.39	158.66	1.67
55.1	117.30	-0.93	127.09	0.07	132.62	-2.07	145.20	-0.48	157.64	1.63
60.1	117.00	-1.01	126.74	0.03	131.98	-2.23	144.41	-0.58	156.69	1.59

Table 13. Calculated isochoric heat capacities C_v (J.mol^{-1}.K^{-1}) of ethanol at different isotherms.

P/MPa	*T*=323.31 K	Deviation (%)	*T*=347.10 K	Deviation (%)	*T*=369.38 K	Deviation (%)	*T*=397.28 K	Deviation (%)	*T*=422.90 K	Deviation (%)
5.1	102.37	0.11	110.50	0.23	117.90	0.32	125.71	-0.17	135.28	2.37
10.1	102.16	0.12	110.23	0.31	117.26	0.24	125.12	0.02	134.25	2.47
15.1	101.97	0.11	109.98	0.37	116.70	0.16	124.55	0.13	133.31	2.47
20.1	101.81	0.10	109.75	0.41	116.21	0.08	124.03	0.18	132.47	2.42
25.1	101.66	0.09	109.55	0.44	115.78	0.00	123.54	0.20	131.73	2.36
30.1	101.52	0.07	109.36	0.46	115.38	-0.06	123.09	0.21	131.07	2.29
35.1	101.39	0.04	109.19	0.48	115.02	-0.13	122.68	0.20	130.48	2.22
40.1	101.28	0.01	109.02	0.49	114.69	-0.20	122.30	0.19	129.94	2.16
45.1	101.17	-0.02	108.87	0.49	114.38	-0.27	121.94	0.17	129.45	2.09
50.1	101.06	-0.05	108.72	0.48	114.08	-0.34	121.59	0.13	129.00	2.02
55.1	100.97	-0.08	108.57	0.47	113.80	-0.41	121.25	0.09	128.56	1.95
60.1	100.88	-0.11	108.43	0.46	113.53	-0.49	120.93	0.05	128.15	1.88

Table 14. Calculated Joule-Thomson coefficients *JT* (K.MPa^{-1}) of ethanol at different isotherms.

P/ MPa	*T*=323.31 K	Deviation (%)	*T*=347.10 K	Deviation (%)	*T*=369.38 K	Deviation (%)	*T*=397.28 K	Deviation (%)	*T*=422.90 K	Deviation (%)
5.1	-0.31422	0.51	-0.26511	0.15	-0.21582	1.53	-0.12720	-2.32	-0.03984	29.84
10.1	-0.32080	0.71	-0.27363	0.11	-0.23034	2.21	-0.12720	-1.19	-0.03984	8.54
15.1	-0.32651	0.89	-0.28086	0.09	-0.24238	2.73	-0.15041	-0.52	-0.07311	3.11
20.1	-0.33155	1.06	-0.28711	0.08	-0.25259	3.15	-0.16877	-0.07	-0.09863	0.80
25.1	-0.33604	1.23	-0.29260	0.09	-0.26139	3.49	-0.18372	0.23	-0.11888	-0.43
30.1	-0.34009	1.39	-0.29747	0.11	-0.26912	3.81	-0.19621	0.48	-0.13543	-1.17
35.1	-0.34376	1.55	-0.30185	0.15	-0.27599	4.09	-0.20686	0.68	-0.14927	-1.65
40.1	-0.34711	1.71	-0.30581	0.20	-0.28217	4.36	-0.21610	0.87	-0.16109	-1.95
45.1	-0.35018	1.86	-0.30942	0.26	-0.28779	4.62	-0.22425	1.07	-0.17135	-2.14
50.1	-0.35299	2.01	-0.31272	0.33	-0.29293	4.88	-0.23152	1.26	-0.18040	-2.22
55.1	-0.35558	2.14	-0.31575	0.40	-0.29765	5.13	-0.23808	1.46	-0.18847	-2.24
60.1	-0.35794	2.27	-0.31853	0.47	-0.30201	5.38	-0.24404	1.66	-0.19575	-2.20

4. Conclusions

The density and the speed of sound in ethanol have been measured simultaneously at a temperature range of (323-423) K and pressure up to 65 MPa. The overall expanded uncertainty of the obtained density and sound velocities were found to be 0.09 % and 0.03 % respectively. Also, the overall % AAD of the measured densities and sound velocities in comparison to Schroeder et al.-EoS were calculated to 0.15 % and 0.30 %, respectively.

The measured sound velocities were used to introduce a Gaussian Process Regression (GPR) model to estimate the speed of sound in ethanol at any (*P*, *T*) of interest. Then, the initial values of the density, sound velocity and isobaric heat capacity at a reference temperature were used to calculate other derived properties at any (*P*, *T*) of interest employing the measured sound velocities. The % AAD of the calculated densities, isobaric and isochoric heat capacities and Joule-Thomson coefficients in comparison with predictions of the Schroeder et al.-EoS were estimated to be 0.06 %, 0.73 %, 0.62 % and 2.22 %. Furthermore, the average uncertainty associated with the derived properties were found to be 0.21 %, 1.01 %, 1.34 % and 0.35 % for density, isobaric heat capacity, isochoric heat capacity and Joule-Thomson coefficient, respectively.

AUTHOR INFORMATION

Corresponding Author

*Tel:+441314513797, Fax:+441314513127 Email:a.chapoy@hw.ac.uk

ORCD ID

https://orcid.org/0000-0002-1368-5091

Notes

The authors declare no competing financial interest.

5. Appendix

5.1 Uncertainty calculations

5.1.1 The uncertainties of temperature measurement

In this setup combined standard uncertainty of temperature measurement was calculated according to:

$$U_c(T) = \sqrt{{u_{system}}^2 + {u_{calibration}}^2 + {u_{repeatability}}^2} \qquad \text{eq. (14)}$$

The system and repeatability standard uncertainties were found to be 0.01 K. Moreover, the calibration function used to convert the actual measured temperature to the calibrated value (in K) was:

$$T_{Calibrated}(T) = 0.00000081T^3 - 0.0008875T^2 + 1.31559927T - 309.544 \qquad \text{eq. (15)}$$

Therefore, $u_{calibration}$ was obtained according to:

$$u_{calibration} = \left|\frac{dT_{Calibrated}}{dT}\right| \times \Delta T \qquad \text{eq. (16)}$$

In this equation, ΔT is equal to 0.01 K and derivative of the calibration function (in K) can be expressed as:

$$\frac{dT_{Calibrated}}{dT} = 3 \times 0.00000081T^2 - 2 \times 0.0008875T + 1.31559927 \qquad \text{eq. (17)}$$

The combined standard uncertainty of temperature measurement, $u_c(T)$, was calculated using eq. (14). This value for all the data points was found to be 0.02 K. Therfore, the expanded uncertainty (with 95 % level of confidence) of the measured temperatures were found to be 0.04 K.

5.1.2 The uncertainties of pressure measurement

A similar method was used to calculate the combined standard uncertainty associated with pressure measurement. The systematic standard uncertainty of the pressure transducer was found from the provided information by the manufacturer (u_s=0.018 MPa) and the standard uncertainty in repeatability of measured pressure in this transducer was found to be 0.002 MPa. Before conducting the measurements, the transducer was calibrated. Employing the calibration formula and its derivative, the standard uncertainty of calibration was found to be 0.001 MPa. Finally, using eq. (14), the combined standard uncertainty and the expanded uncertainty (with 95 % level of confidence) in pressure measurement was found to be 0.018 MPa and 0.036 MPa respectively.

5.1.3 The uncertainties of density measurement

For the density measurement the combined standard uncertainty was calculated using the following equation:

$$U_c(\rho) = \sqrt{\left(\frac{\mathrm{d}\rho}{dT} \times u_T\right)^2 + \left(\frac{\mathrm{d}\rho}{dP} \times u_P\right)^2 + {u_{system}}^2 + {u_{calibration}}^2 + {u_{ref.}}^2 + {u_{repeatability}}^2}$$

eq. (18)

As calculated before, the combined standard uncertainty of pressure, $u_c(\mathrm{p})$, and temperature, $u_c(\mathrm{T})$, were 0.018 MPa and 0.02 K, respectively. Moreover, the density gradient due to the temperature and pressure were estimated employing the Schroeder et al.- EoS. Moreover, based on the manufacturer information, the uncertainity of repeatability and the uncertainty of the system were found to be 0.01($\frac{kg}{m^3}$) and 0.1 ($\frac{kg}{m^3}$), respectively.

The calibration uncertainty was achieved from the equation used to calculate the sample density for each isotherm;

$$\rho_s = (\tau_s^2 - \tau_{N_2}^2) \times \left[\frac{\rho_{H_2O} - \rho_{N_2}}{\tau_{H_2O}^2 - \tau_{N_2}^2}\right] + \rho_{N_2} \qquad \text{eq. (19)}$$

The uncertainty of the calibration equation was given by:

$$\mathrm{u}(\rho)_{calibration} = \left|\frac{d\rho}{dP}\right| \times \Delta P \qquad \text{eq. (20)}$$

Where,

$$\frac{d\rho}{dP} = \frac{d\left[\tau_s^2 - \tau_{N_2}^2\right]}{dp} \times \left(\frac{\rho_{H_2O} - \rho_{N_2}}{\tau_{H_2O}^2 - \tau_{N_2}^2}\right) + \frac{d\left[\frac{\rho_{H_2O} - \rho_{N_2}}{\tau_{H_2O}^2 - \tau_{N_2}^2}\right]}{dp} \times \left(\tau_s^2 - \tau_{N_2}^2\right) + \frac{d\rho_{N2}}{dP}$$

$$= -2\tau_{N_2}\frac{d\tau_{N_2}}{dp} \times \left(\frac{\rho_{H_2O} - \rho_{N_2}}{\tau_{H_2O}^2 - \tau_{N_2}^2}\right) + \frac{\frac{d\left[\rho_{H_2O} - \rho_{N_2}\right]}{dp} \times \left(\tau_{H_2O}^2 - \tau_{N_2}^2\right) - \frac{d\left[\tau_{H_2O}^2 - \tau_{N_2}^2\right]}{dp} \times \left(\rho_{H_2O} - \rho_{N_2}\right)}{\left(\tau_{H_2O}^2 - \tau_{N_2}^2\right)^2}$$

$$\times \left(\tau_s^2 - \tau_{N_2}^2\right) + \frac{d\rho_{N2}}{dP}$$

eq. (21)

The derivatives of the oscillation periods of water and nitrogen were found using the fitted equation on the measured data points. Also, the reference equations of state for nitrogen [47] and water [46] were used to find the derivatives of densities with respect to temperature. The reported maximum uncertainties of the reference densities of water and nitrogen in the (*P*, *T*) range of this work are 0.01 % and 0.05 %, respectively. For all the measured densities of this work, the maximum effect of reference densities uncertainties on the final result ($u_{ref.}$) was found to be less than 3 mol.m^{-3}. Moreover, ΔP is the uncertainty in the measurement of P which was equal to 0.018 MPa. The values of the density derivatives of ethanol with respect to temperature and pressure were estimated employing the predictive model of Schroeder et al.-EoS . Finally, the estimated expanded uncertainty with 95 % level of confidence was calculated from following equation:

$$U(\rho) = 2 \times u_c(\rho) \qquad \text{eq. (22)}$$

5.1.4 The uncertainties of the speed of sound measurement

The expanded uncertainty (with 95 % level of confidence) of the measured speed of sound in ethanol was obtained using the measured reflection time (t_r) of the sound waves in the fluid and the measured path length (*L*) of the acoustic cell at each (*P*, *T*) of interest employing the below equation;

$$v = \frac{L}{t_r} \implies u(v) = \Delta v = v \times \sqrt{\left(\frac{\Delta L}{L}\right)^2 + \left(\frac{\Delta t_r}{t_r}\right)^2} \qquad \text{eq. (23)}$$

At each isotherm, the path length of the sound wave was calculated using a linear function of pressure (L=f (p)) found in the calibration. This function was found by fitting the measured internal length of the acoustic cell to a linear function of pressure for the reference substance (water). Therefore, the standard uncertainty of the calibrated internal length is calculated using the standard uncertainty of regression and the standard uncertainty associated with predicted speed of sound in the water (maximum uncertainty = 0.2 %[46]). The procedure of the standard uncertainty calculation for a linear regression can be found in the literature. Therefore, assuming a 0.2 % standard uncertainty of the speed of sound in water[46], the maximum standard uncertainty of the calibrated internal length ($\Delta L_{cal.}$) was found to be 1.00482×10^{-5}m.

The function found in the calibration section was then used to determine the internal length ($L_{meas.}$) at different pressures of the experiment. Therefore, the standard uncertainty of the length measurement during the main measurements was found by:

$$L = f(p) \implies \Delta L_{meas.} = \left|\frac{d\,f(p)}{dp}\right| \times \Delta p \qquad \text{eq. (24)}$$

Therefore, combined standard uncertainty of length measurement was found to be:

$$u_c(L) = \Delta L = \sqrt{{\Delta L_{meas.}}^2 + {\Delta L_{Cal.}}^2} \qquad \text{eq. (25)}$$

The standard uncertainty of the measured reflection time, was found using the standard uncertainty of time measurement in the oscilloscope. Also, the standard uncertainty of the repeatability, $u_{repeatability}$, in the measured sound velocities was measured by repeating the measurements for a single (*P, T*). The standard deviation of the measured sound velocities was reported as the standard uncertainty in repeatability of the results. For all the measurements $u_{repeatability}$ was found to be 0.11 m/s. Furthermore, the effects of the uncertainties associated with temperature and pressure measurements on the measured sound velocities were investigated. Although the effect of temperature change on the uncertainty of the measured sound velcity ($\frac{\mathrm{d}SOS}{dT} \times u_T$) was insignificant, the uncertainties associated with pressure changes ($\frac{\mathrm{d}SOS}{dP} \times u_P$) could not be ignored in the uncertainty calculations.

Finally, the expanded uncertainty (with 95 % level of confidence, *k*=2) of the measured sound velocities was calculated by:

$$U(v) = 2 \times u_c(v) = 2 \times \sqrt{\left(\left|\frac{\mathrm{d}SOS}{dP}\right| \times u_P\right)^2 + {u_{repeatability}}^2 + {u_{calibration/sysetm}}^2}$$

eq. (26)

5.1.5 The uncertainties of the derived properties

As explained before, in this work the measured sound velocities were used to obtain derived properties. Also, to simplify the estimation of sound velocities at any (*P, T*) of interest, a GPR model was used. Using this model, the speed of sound in ethanol can be estimated for any pressure and temperature within the (*P, T*) range of this work. The maximum combined standard uncertainty of the predicted sound velocities (using the GPR model) was found to be 4.44 m.s^{-1}. Therefore, to estimate the standard uncertainties of the derived properties, values of each property were calculated considering the maximum deviation in the estimated sound velocities. For instance, at any (*P, T*) of interest three values of the isobaric heat capacity was

determined using three values of the speeds of sound. The first value of the C_p was determined using the *SoS* predicted with the GPR model. This value of the C_p was the main result. The second and third values of the C_p were calculated assuming the *SoS* to be (*SoS*+4.44) $m.s^{-1}$ and (*SoS*-4.44) $m.s^{-1}$, respectively. Then, the maximum deviations of the second and third calculated C_p from the main result (the first C_p) was reported as the standard uncertainty of the C_p at this point.

Similar calculation was performed for all properties. The overall relative uncertainty of the calculated density, isobaric heat capacity, isochoric heat capacity and Joule-Thomson coefficient were found to be 0.21 %, 1.01 %, 1.34 % and 0.35 %.

6. References

1. Mann, L. B.; Folts, J. D., Effects of ethanol and other constituents of alcoholic beverages on coronary heart disease: a review. *Pathophysiology* **2004,** *10*, 105-112.
2. Irvine, L. F., Relevance of the developmental toxicity of ethanol in the occupational setting: a review. *J. Appl. Toxicol.* **2003,** *23*, 289-299.
3. Hansen, A. C.; Zhang, Q.; Lyne, P. W., Ethanol–diesel fuel blends—a review. *Bioresour. Technol.* **2005,** *96*, 277-285.
4. Shulman, A.; Wolf, R., Alcohol ingestion, hormonal changes, and the skin. *Clinics in dermatology* **1999,** *17*, 405-409.
5. Dillon, H.; Penoncello, S., A fundamental equation for calculation of the thermodynamic properties of ethanol. *Int. J. Thermophys.* **2004,** *25*, 321-335.
6. Schroeder, J.; Penoncello, S.; Schroeder, J., A Fundamental Equation of State for Ethanol. *J. Phys. Chem. Ref. Data* **2014,** *43*, 043102.
7. Wegge, R.; Richter, M.; Span, R., Speed of sound measurements in ethanol and benzene over the temperature range from (253.2 to 353.2) K at pressures up to 30 MPa. *J. Chem. Eng. Data* **2015,** *60*, 1345-1353.
8. Dzida, M.; Żak, A.; Ernst, S., Thermodynamic and acoustic properties of binary mixtures of alcohols and alkanes. I. Speed of sound in (ethanol+n-heptane) under elevated pressures. *J. Chem. Thermodyn.* **2005,** *37*, 405-414.
9. Sun, T.; Ten Seldam, C.; Kortbeek, P.; Trappeniers, N.; Biswas, S., Acoustic and Thermodynamic Properties of Ethanol from 273.15 to 333.1 5 K and up to 280 MPa. *Phys. Chem. Liq.* **1988,** *18*, 107-116.
10. Vega-Maza, D.; Martín, M. C.; Trusler, J. M.; Segovia, J. J., Heat capacities and densities of the binary mixtures containing ethanol, cyclohexane or 1-hexene at high pressures. *J. Chem. Thermodyn.* **2013,** *57*, 550-557.
11. Miyazawa, T.; Kondo, S.; Suzuki, T.; Sato, H., Specific heat capacity at constant pressure of ethanol by flow calorimetry. *J. Chem. Eng. Data* **2012,** *57*, 1700-1707.
12. Fulem, M.; Růžička, K.; Růžička, V., Heat capacities of alkanols: Part I. Selected 1-alkanols C2 to C10 at elevated temperatures and pressures. *Thermochim. Acta* **2002,** *382*, 119-128.
13. Sun, T.; Schouten, J.; Biswas, S., Determination of the thermodynamic properties of liquid ethanol from 193 to 263 K and up to 280 MPa from speed-of-sound measurements. *Int. J. Thermophys.* **1991,** *12*, 381-395.
14. Young, S. In *The vapour-pressures, specific volumes, heats of vaporisation, and critical constants of thirty pure substances*, Proc. R. Dublin Soc, 1910; pp 374-444.
15. Tammann, G.; Rühenbeck, A., Die spezifischen Volumen des Wassers zwischen 20° und 650°, die des Äthyläthers und des Äthylalkohols zwischen 20° und 400° bei Drucken von 1-2500 kg/cm2. *Annalen der Physik* **1932,** *405*, 63-79.
16. Gupta, A. C.; Hanks, R. W., Liquid phase PVT data for binary mixtures of toluene with nitroethane and acetone, and benzene with acetonitrile, nitromethane, and ethanol. *Thermochim. Acta* **1977,** *21*, 143-152.
17. Yusa, M.; Mathur, G. P.; Stager, R. A., Viscosity and compression of ethanol-water mixtures for pressures up to 40,000 psig. *J. Chem. Eng. Data* **1977,** *22*, 32-35.
18. Ozawa, S.; Ooyatsu, N.; Yamabe, M.; Honmo, S.; Ogino, Y., Specific volumes of binary liquid mixtures at high pressures I. Experimental results for (ethanol+ methylcyclopentane),(n-heptane+ ethanol), and (methylcyclopentane+ n-heptane). *J. Chem. Thermodyn.* **1980,** *12*, 229-242.
19. Golub'ev, I. F. V. k., T.N.;Zolin,V.S., Experimental research on density of aliphatic alcohols at different temperatures and pressures *Inzh. Fiz. Zh.* **1980,** *38*, 668.

20. Benson, G. C.; D'Arcy, P. J., Excess isobaric heat capacities of water-n-alcohol mixtures. *J. Chem. Eng. Data* **1982,** *27*, 439-442.
21. Sauermann, P. Pressure-density-temperature measurements on pure trifluoroethanol, ethanol, n-hexane and equimolar mixture n-hexane - ethanol. Germany, 1992.
22. Sauermann, P.; Holzapfel, K.; Oprzynski, J.; Kohler, F.; Poot, W.; de Loos, T. W., The pϱT properties of ethanol+ hexane. *Fluid Phase Equilib.* **1995,** *112*, 249-272.
23. Takiguchi, Y.; Uematsu, M., PVT Measurements of Liquid Ethanol in the Temperature Range from 310 to 363 K at Pressures up to 200 MPa. *Int. J. Thermophys.* **1995,** *16*, 205-214.
24. Takiguchi, Y.; Uematsu, M., Densities for liquid ethanol in the temperature range from 310 K to 480 K at pressures up to 200 MPa. *J. Chem. Thermodyn.* **1996,** *28*, 7-16.
25. Watts, L.; Louie, B., Apparatus for measuring vapor-liquid equilibria and phase densities of complex aqueous solutions. *Int. J. Thermophys.* **2000,** *21*, 1139-1151.
26. Kitajima, H.; Kagawa, N.; Tsuruno, S., Endo Measurement of Isochoric Specific Heat Capacity for Pure Alcohol with Adiabatic Twin-Cell Calorimeter. *Trans. Jpn. Soc. Mech. Eng., Ser. B* **2003,** *69*, 1921-1927.
27. Pečar, D.; Doleček, V., Volumetric properties of ethanol–water mixtures under high temperatures and pressures. *Fluid Phase Equilib.* **2005,** *230*, 36-44.
28. Zéberg-Mikkelsen, C. K.; Andersen, S. I., Density measurements under pressure for the binary system 1-propanol+ toluene. *J. Chem. Eng. Data* **2005,** *50*, 524-528.
29. Watson, G.; Zéberg-Mikkelsen, C. K.; Baylaucq, A.; Boned, C., High-pressure density measurements for the binary system ethanol+ heptane. *J. Chem. Eng. Data* **2006,** *51*, 112-118.
30. Matkowska, D.; Gołdon, A.; Hofman, T., Densities, excess volumes, isobaric expansivities, and isothermal compressibilities of the 1-ethyl-3-methylimidazolium ethylsulfate+ ethanol system at temperatures (283.15 to 343.15) K and pressures from (0.1 to 35) MPa. *J. Chem. Eng. Data* **2009,** *55*, 685-693.
31. Gonçalves, F.; Trindade, A.; Costa, C.; Bernardo, J.; Johnson, I.; Fonseca, I.; Ferreira, A., PVT, viscosity, and surface tension of ethanol: New measurements and literature data evaluation. *J. Chem. Thermodyn.* **2010,** *42*, 1039-1049.
32. Torcal, M.; Teruel, M. I.; García, J.; Urieta, J. S.; Mainar, A. M., P ρ T Measurements of the (Ethanol+ Linalool),(Propan-1-ol+ Linalool), and (Propan-2-ol+ Linalool) Mixtures: Cubic and Statistical Associating Fluid Theory-Based Equation of State Analyses. *J. Chem. Eng. Data* **2010,** *55*, 5332-5339.
33. Sommer, D.; Kleinrahm, R.; Span, R.; Wagner, W., Measurement and correlation of the (p, ρ, T) relation of liquid cyclohexane, toluene, and ethanol in the temperature range from 233.15 K to 473.15 K at pressures up to 30MPa for use as density reference liquids. *J. Chem. Thermodyn.* **2011,** *43*, 117-132.
34. Kariznovi, M.; Nourozieh, H.; Abedi, J., Experimental measurements and predictions of density, viscosity, and carbon dioxide solubility in methanol, ethanol, and 1-propanol. *J. Chem. Thermodyn.* **2013,** *57*, 408-415.
35. Duarte, P.; Silva, M.; Rodrigues, D. i.; Morgado, P.; Martins, L. F.; Filipe, E. J., Liquid mixtures involving hydrogenated and fluorinated chains:(p, ρ, T, X) surface of (ethanol+ 2, 2, 2-trifluoroethanol), Experimental and Simulation. *J. Phys. Chem. B* **2013,** *117*, 9709-9717.
36. Martínez-López, J. F.; Mainar, A. M.; Urieta, J. S.; Pardo, J. I., Thermophysical properties of {R-fenchone+ ethanol} at several temperatures and pressures. *J. Chem. Thermodyn.* **2014,** *69*, 48-55.
37. Brown, J.; Slutsky, L.; Nelson, K.; Cheng, L.-T., Velocity of sound and equations of state for methanol and ethanol in a diamond-anvil cell. *Science* **1988,** *241*, 65-68.
38. Carnevale, E.; Litovitz, T., Pressure dependence of sound propagation in the primary alcohols. *J. Acoust. Soc. Am* **1955,** *27*, 547-550.

39. Dzida, M.; Marczak, W., Thermodynamic and acoustic properties of binary mixtures of alcohols and alkanes. II. Density and heat capacity of (ethanol+n-heptane) under elevated pressures. *J. Chem. Thermodyn.* **2005,** *37*, 826-836.
40. Hawley, S.; Allegra, J.; Holton, G., Ultrasonic-Absorption and Sound-Speed Data for Nine Liquids at High Pressures. *J. Acoust. Soc. Am* **1970,** *47*, 137-143.
41. Walsh, J. M.; Rice, M. H., Dynamic compression of liquids from measurements on strong shock waves. *The Journal of Chemical Physics* **1957,** *26*, 815-823.
42. Eden, H.; Richardson, E., The propagation of ultrasonics in organic liquids under pressure. Variation of specific heat ratio and viscosity with pressure. *Acta Acust. Acust.* **1960,** *10*, 309-315.
43. Wilson, W.; Bradley, D., Speed of sound in four primary alcohols as a function of temperature and pressure. *J. Acoust. Soc. Am* **1964,** *36*, 333-337.
44. Ohmori, T.; Kimura, Y.; Hirota, N.; Terazima, M., Thermal diffusivities and sound velocities of supercritical methanol and ethanol measured by the transient grating method. *Phys. Chem. Chem. Phys.* **2001,** *3*, 3994-4000.
45. Ahmadi, P.; Chapoy, A.; Tohidi, B., Density, speed of sound and derived thermodynamic properties of a synthetic natural gas. *J. Nat. Gas Sci. Eng.* **2017,** *40*, 249-266.
46. Wagner, W.; Pruß, A., The IAPWS formulation 1995 for the thermodynamic properties of ordinary water substance for general and scientific use. *J. Phys. Chem. Ref. Data* **2002,** *31*, 387-535.
47. Span, R.; Lemmon, E. W.; Jacobsen, R. T.; Wagner, W.; Yokozeki, A., A reference equation of state for the thermodynamic properties of nitrogen for temperatures from 63.151 to 1000 K and pressures to 2200 MPa. *J. Phys. Chem. Ref. Data* **2000,** *29*, 1361-1433.
48. Hirschfelder, J.; Bird, R. B.; Curtiss, C. F., Molecular theory of gases and liquids. **1964**.
49. Trusler, M., *Physical acoustics and metrology of fluids*. Taylor & Francis Group: Great Britain, 1991.
50. Fazelabdolabadi, B.; Bahramian, A., Acoustic determination of the heavy oil thermophysical properties: Thermodynamic consistency revisited. *Fuel* **2012,** *102*, 49-53.
51. Rasmussen, C. E.; Williams, C. K., *Gaussian processes for machine learning*. MIT press Cambridge: 2006; Vol. 1.
52. Kennedy, M. C.; O'Hagan, A., Bayesian calibration of computer models. *J R Stat Soc Series B Stat Methodol* **2001,** *63*, 425-464.